Granular Matter (2025) 27:55
https://doi.org/10.1007/s10035-025-01531-w

RESEARCH

Tuning geometry in staple-like entangled particles: "pick-up" experiments and Monte Carlo simulations

Youhan Sohn[1] · Saeed Pezeshki[1] · Francois Barthelat[1]

Received: 1 December 2024 / Accepted: 25 April 2025

Abstract
Entangled matter provides intriguing perspectives in terms of deformation mechanisms, mechanical properties, assembly and disassembly. However, collective entanglement mechanisms are complex, occur over multiple length scales, and they are not fully understood to this day. In this report, we propose a simple pick-up test to measure entanglement in staple-like particles with various leg lengths, crown-leg angles, and backbone thickness. We also present a new "throw-bounce-tangle" model based on a 3D geometrical entanglement criterion between two staples, and a Monte Carlo approach to predict the probabilities of entanglement in a bundle of staples. This relatively simple model is computationally efficient, and it predicts an average density of entanglement which is consistent with the entanglement strength measured experimentally. Entanglement is very sensitive to the thickness of the backbone of the staples, even in regimes where that thickness is a small fraction (<0.04) of the other dimensions. We finally demonstrate an interesting use for this model to optimize staple-like particles for maximum entanglement. New designs of tunable "entangled granular metamaterials" can produce attractive combinations of strength, extensibility, and toughness that may soon outperform lightweight engineering materials such as solid foams and lattices.

Keywords Entangled matter · Granular metamaterials · U-shape particles · Monte Carlo simulations

1 Introduction

Typical granular materials made of spherical or quasi-spherical grains require mechanical confinement to generate shear strength [1–3] or a cohesive second phase at the interface between the grains [4, 5]. Grains with more extreme geometries such as elongated rods can assemble into free standing structures with some tensile strength, because of long range interactions and multiple contact points [6–9]. Long rods, in turn, may be assembled into hexapods [10] or other star-like particles with entanglement or "geometric cohesion" [11], offering intriguing possibilities in terms of structural design and architecture [12, 13]. Even more extreme designs have branches with hooks and barbs, with the classical example of U-shape staple-like particles [14–17]. These particles can indeed latch and hook onto one another, generating substantial tensile strength [15, 18, 19]. Tensile force chains develop in these materials [16], and although they tend to be more sparse than typical compressive chains, they are sufficiently strong and stable to enable free-standing structures (beams, columns [14, 20]). How the shapes of these particles govern entanglement, and in turn translate into strength provides a rich landscape in terms of mechanics and design. For example, geometrical alteration on standard staples, such as changing the length of legs [14] twisting of the legs [20, 21], or actively change the shape of the particles [22] have been shown to have profound impact on entanglement and strength, and interestingly, optimum geometries have already been identified within these design spaces [14, 20, 21]. Various experimental approaches have been used to assess entanglement strength. Perhaps the simplest of these experiments consists of assessing the size of an entangled bundle of particles that can be lifted by just picking up a few staples against gravity [6, 9, 20]. More complex experiments have measured angle of repose [16], and the stability of long free-standing columns [23] and short columns subjected to vibrations [14]. Other mechanical tests on

✉ Francois Barthelat
francois.barthelat@colorado.edu

1 Department of Mechanical Engineering, University of Colorado, 427 UCB, 1111 Engineering Dr, Boulder, CO 80309, USA

Published online: 19 May 2025

entangled materials have included tensile tests [15, 19] and flexural tests [20]. While these experiments have provided "macroscopic" mechanical properties for bundles of entangled particles, they provide limited insights into the fundamental mechanisms of entanglement and disentanglement at the local level. In addition, each of these experimental approaches was used to explore only one particular aspect of particle design (for example, [14] focused on the effect of leg length only). The lack of "unified" testing methods makes it difficult to assess and compare the entanglement efficacy of staples with different designs. To gain insights into the mechanics of entanglement, numerical models were also developed, primarily based on the discrete element method (DEM) [24]. These models have revealed the effect of packing density on entanglement strength [14], the impact of alignment of staple-like particles across gravity [20], the dynamic structure of tensile force lines [16, 19, 25] or the shifting properties of particles where entanglement can be tuned with dynamic shape change [22]. However, these DEM models, performed on hundreds or thousands of particles with complex shapes, can be computationally expensive and produce large amounts of data that can be difficult to interpret. In this report, we present a relatively simple experiment to measure entanglement based on a bundle pick-up method. The second part of the report presents an entanglement model based on a pair of staples. A simple geometrical criterion for geometrical entanglement, together with a Monte Carlo approach, produces a prediction for entanglement probability and the volumetric density of entangled particles that agree well with experiments on staples with a variety of designs.

2 Experiments

Our objective was to provide a simple and repeatable protocol to measure the entanglement and strength of various staple-like particle geometries. In consistency with previous studies, we assumed that the extent, or density, of entanglement in a bundle is reflected by its strength, whether it is measured by stability under mechanical vibration [14], flexural tests [20], tensile tests [19] or as recently demonstrated on active entangled matter [22]. The base particles we used for this study were standard steel office staples (Swingline, IL), with dimensions shown in Fig. 1a. In the rest of this report, we will use the same terminology as in the staple industry: The center section is referred to as "crown", and the two branches are referred to as "legs". These staples come in the form of "sticks" of about 200 staples, bonded by a relatively weak polymeric adhesive. To separate individual staples, we immersed sticks of staples in acetone, which immediately dissolved the adhesive and detached the staples. After thorough cleaning and drying, bundles of staples were prepared for the pick-up test. A thousand staples were first pluviated into a container with the shape of a truncated cone, with a base diameter of 80 mm (approximately 6.3 times the length of the crown of individual staples, Fig. 1b), and from a height of 200 mm from the container. Next, we used a custom tool made of three staples embedded at the end of a 3D printed handle (Fig. 1c) to pick up staples from the container. The tip of the tool was first directed towards the center of the surface of the bundle, with a tilt angle of about 30° from the vertical. As the tip of the tool contacted the surface, the tool was straightened to a vertical position to engage 3 to 5 staples near the surface. The tool was finally gently pulled upwards and against gravity at a rate of about 40 mm/s (Fig. 1d). The pickup process was dominated by gravity forces and by entanglement forces between staples and in comparison, the exact force produced by the pick-up tool on the topmost staples were less relevant. The number

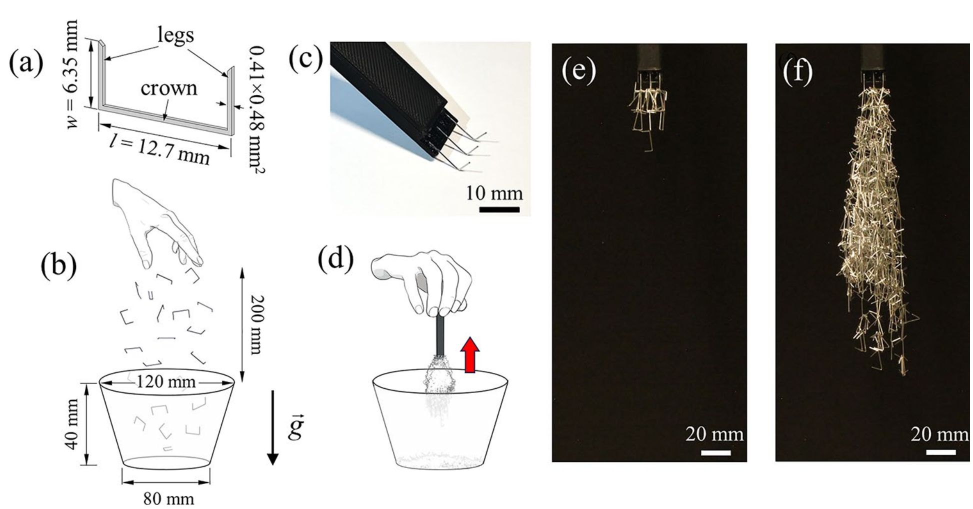

Fig. 1 Overview of the "pick-up" experiment: **a** Individual standard office staple with dimensions; These staples are **b** poured into an open container. **c** A custom "fishing tool" was used to **d** grab the center staples and pull upwards. The amount of picked-up staples was a strong function of geometry and could be **e** small (a few staples) to **f** large (most of the staples picked up)

of staples picked up by this process depends on how much entanglement is present in the bundle, which itself is a strong function of the geometry of the individual staples. Some geometries led to poor entanglement and few staples picked up (Fig. 1e), while other geometries generated more entanglement and much larger groups of picked-up staples (Fig. 1f). To quantify the entanglement of staples, we used a "picked-up fraction," which we defined as the fraction of staples lifted from the initial bundle of 1000 staples (measured by weighing the staples picked from the bundle). Repeated tests on the same staples revealed typical variations of 5–10% around the mean value of the picked-up fraction. This repeatability was sufficient to discriminate between different staple geometries.

We now present the first part of the study, where we varied the angle between the legs and the crown of the individual staples (the crown-leg angle θ). We designed and fabricated 3D-printed tools to fold the legs to either decrease or increase θ from $\theta=90°$ reference sticks of staples (Fig. 2a). We then performed three pick-up experiments on each of these geometries. Figure 2b shows the pick-up fraction as

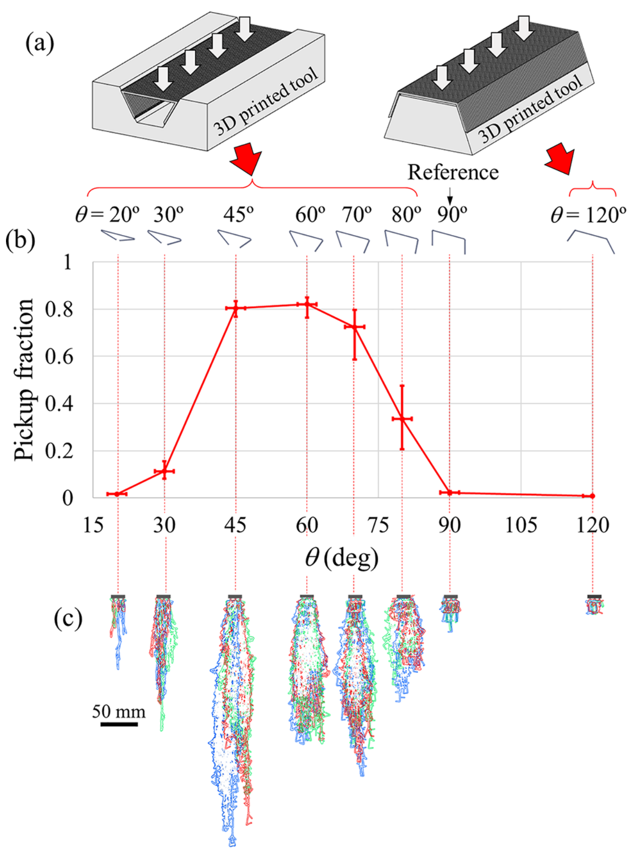

Fig. 2 **a** The crown-leg angle of individual staples can be increased or decreased from the $\theta=90°$ reference using custom 3D printed embossing tools [19]; **b** Experimental pick-up fraction as a function of crown-leg angle θ. Horizontal error bars reflect the variability of angle θ, and vertical error bars reflect the range of pickup fraction measured for each geometry; **c** Composite images of the picked-up bundles

a function of the crown-leg angle θ, together with three superimposed contours of the picked-up bundle (Fig. 2c). These contours were obtained by extracting the outer contour of the bundle from pictures acquired during the pick-up experiments. The contours were then superimposed, using a different color for each of the three experiments. The reference staples produced a modest entanglement, with an average pick-up fraction of only about 0.03. As expected, this number was even smaller for high angles ($\theta=120°$). On the other hand, decreasing θ greatly improved entanglement, with a pick-up fraction greater than 0.8 for $\theta=60°$. An intuitive explanation is that decreasing θ turns the staples into a pair of increasingly sharp "hooks," which can generate more robust entanglement with other staples. However, decreasing the angle further led to poorer entanglement, with a pick-up fraction of less than 2% for $\theta=20°$. We hypothesized that another effect is at play: The reduction of θ in effect "closes" the geometry of the staple, reducing the probability of the staples to geometrically "engage" with one another. The observed entanglement peak $\theta=45$–$60°$ would then be the result of two competing mechanisms: closing θ makes the entanglement between two staples stronger once they engage, but closing θ also decreases the probability of staples mutually engaging. In the following sections, we introduce a simple model that captures the competition of these mechanisms.

3 A "throw-bounce-tangle" model for geometric entanglement

Entanglement and disentanglement are complex processes that involve multiple spatial and time scales [15, 16, 26]. In this study, we sought a relatively simple model to capture entanglement at a fundamental level, i.e., between two staples, based on geometry only. We assumed a round cross section for the backbone of the staples (with diameter $d=0.45$ mm for a standard office staple) with semi-spherical caps at the ends of the legs (Fig. 3a). This simplification streamlined 3D calculations for staple-to-staple distance, the evaluation of collisions, and other staple-staple interactions.

3.1 Excluded volume and packing fraction

The excluded volume is the statistical volume occupied by individual staples in a randomly distributed bundle of particles, and as seen below it governs the volumetric density of staples [6, 26] We computed the excluded volume of individual staples using Monte Carlo simulations, following Gravish et al. [26]. We first considered a center staple (staple 1) and a spherical volume V centered on that staple with a radius several times the size of the staple. We then

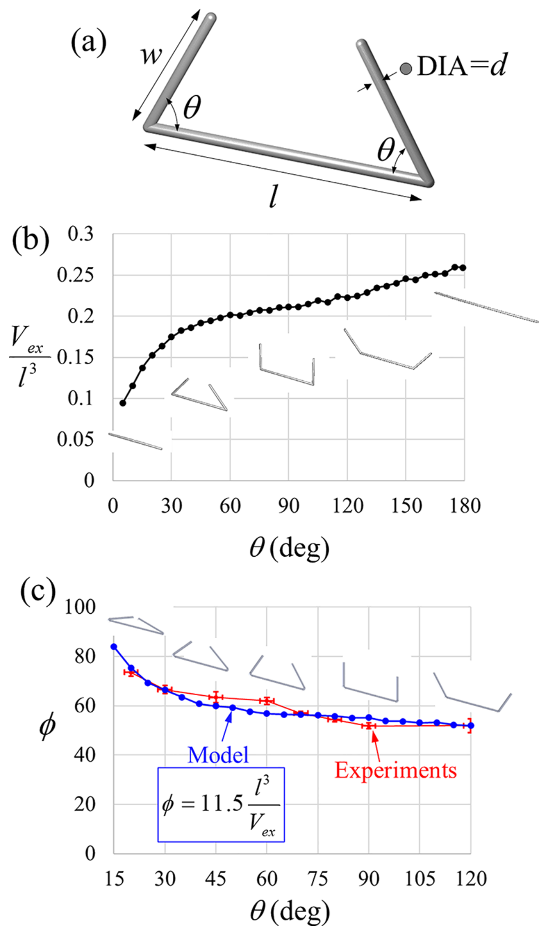

Fig. 3 **a** Geometry of the staples used in the MC models; **b** Nondimensional excluded volume and **c** experimental and modeled volumetric density of staples as a function of crown-leg angle θ

generated a second staple (staple 2) within that volume, at random position and orientation. The occurrence of collisions between staple 1 and 2 was then computed, accounting for the relative position of staple 1 and 2 and the diameter of the backbone. The probability of collision between the two staples is therefore c/N where c is the total number of collisions over N realizations. The excluded volume is simply given by:

$$V_{ex} = \frac{c}{N}V \tag{1}$$

If N is sufficiently large ($N > 10^6$ in our simulations), we found that the result V_{ex} is independent of the simulation volume V. The model was implemented using MATLAB with parallel processing [27]. Using this model, we recovered the theoretically excluded volume of rods of different aspect ratios [6] and the excluded volume of staples with varying leg lengths [26]. Figure 3b shows the results of the excluded volume of standard office staples ($w/l = 0.5$, $d/l = 0.035$) as a function of crown leg angle θ. Staples with higher excluded volumes take more space in the bundle, which results in lower packing factors. More specifically, using previous results on random packing of rods [6] and staples [26], the packing factor (PF) of a bundle of staples can be written:

$$PF = C\frac{V_p}{V_{ex}} \tag{2}$$

where V_p is the volume of the individual staple and C is a constant parameter that corresponds to the average number of staples in contact with a given staple. PF represents the volume fraction of "solid material" in the bundle (Eq. (2) is also known as the random contact model [6]). As opposed to porous or cellular material whose properties are a strong function of solid volume fraction, in bundles of staples it is the number of staples per unit volume, or volumetric staple density ϕ, which is important for strength. It is written:

$$\phi = \frac{l^3}{V_p}PF = C\frac{l^3}{V_{ex}} \tag{3}$$

Note that to keep the results nondimensional, ϕ is written as the average number of staples in a $l \times l \times l$ volume (i.e., the unit volume is expressed in unit of l). To calibrate the constant C, we experimentally measured the staple volume fraction ϕ by pouring 1000 staples into a transparent acrylic container with a circular section (diameter = 38 mm). The height of the bundle of staples in the container was used to compute the volume occupied by the bundle, which was then used to determine the experimental staple volume fraction ϕ. For each geometry, the test was repeated three times and the error on ϕ was relatively small (in the order of 3%). Figure 3c shows ϕ as function of crown-leg angle θ, showing a decrease from about 75 to 50 as θ is increased from $\theta = 20°–120°$. Using the crown length l and V_{ex} computed above for each geometry (Eq. 1), Eq. (3) was fitted onto the experimental volume fraction using C as nondimensional fitting parameter. This process produced $C \approx 11.5$ which is close, but slightly larger than the value of $C \approx 8.75$ obtained through oscillatory excitation on staples by Gravish et al. [14] and larger than for rods [6].

3.2 Modeling entanglement with the throw-bounce-tangle model

The aim of the "throw-bounce-tangle" model we present here was to predict the probability of entanglement of a pair of staples-like particles based on their geometry. The model is centered on a staple (staple 1) which remains stationary. Another staple (staple 2) is placed at a random position on a sphere of fixed radius centered on staple 1, and at a random orientation (Fig. 4a). In this model, the radius of that sphere reflects the typical distance between staples in the bundle, and for this reason, we used the "excluded radius" computed from the excluded volume:

$$R_{ex} = \sqrt[3]{\frac{3}{4\pi} V_{ex}} \tag{4}$$

Initial conformations where staples 1 and 2 collide are not permitted and were rejected. Next, we considered a "throw" step that simulates pouring or vibrations, which would provide an impulse of displacement to staple 2. We considered all possible 3D directions for a translation of staple 2 from the initial position, which can lead to one of two outcomes: Either Staple 2 collides with particle 1, or staple 2 "misses" particle 1. In our algorithm, we considered all possible directions for an impulse on staple 2, in the form of a total solid angle $\boldsymbol{\Omega}=4\pi$. Using simple 3D geometrical rules, we then computed, numerically, a "visibility" solid angle $\boldsymbol{\Omega}^{(v)}$ which led staple 2 to geometrically intersect with staple 1 (Fig. 4a). This process of random placement of staple 2 on the excluded sphere and calculation of the visibility solid angle was repeated N times, so that the probability of staple 2 and 1 to interact was given by:

$$p_v = \frac{1}{N} \sum_{i}^{N} \frac{\Omega_i^{(v)}}{4\pi} \tag{5}$$

The probability p_v therefore provides a measure of how statistically "visible" each staple is to neighboring staples. A

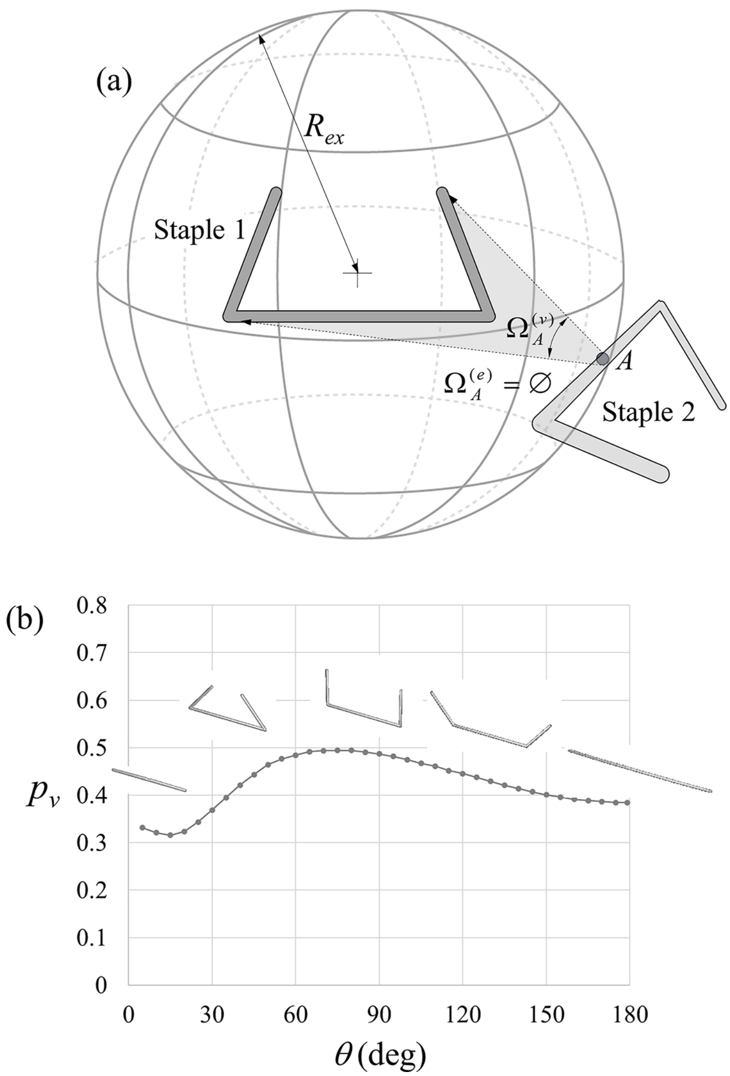

Fig. 4 Diagrams illustrating the throw-bounce-tangle model: **a** Visibility of center staple 1 from staple 2 at a position A on the exclusion sphere. Staple 2 cannot engage staple 1 from position A; **b** statistical "visibility", or probability p_v of individual staples as a function of crown-leg angle θ; **c** In this case staple 2 can engage staple 1 from position B; **d** 2D Diagram showing how a bounce is considered, and a possible further entanglement is assessed (see text for further details)

plot of p_v as a function of crown-leg angle θ (Fig. 4b) shows that p_v is the lowest when legs and crown are aligned, so the staples are effectively rods (cases $\theta=0°$ and $\theta=180°$). Next, a director vector was randomly selected from the solid angle sector $\Omega^{(v)}$. We computed the displacement required for staple 2 to contact staple 1 along that director angle, and we updated the positions of staple 1 and 2, now in contact with each other (see supplemental movie). The interaction of two staples by direct contact does not, however, guarantee that they will entangle. In the example of Fig. 4a, staple 2 can contact staple 1 after a translation from point A. However, none of the contact conformations can lead to entanglement, because the conformations are such that staple 1 and 2 interact like simple rods. To generate entanglement the staples first need to engage, that is they need to enter a conformation where the geometrical hindrance from the concave features of the staples becomes prominent. To capture this effect, we considered regions of the staples that can potentially partially enclose or geometrically "trap" branches from other staples. In this study we considered two of these "nets" region, as shown on Fig. 4c. Each of the nets is a plane triangular region defined by the middle point of the crown, the elbow between crown and leg, and the tip of the leg. Defining a single, larger net enclosed by the crown and both legs was another possibility. However we required the nets to be planar region, and this single net definition was not compatible with the twisted staples we considered below. The staples may also be interpreted as particles made of two adjoined hook-like features, each being able to entangle with neighboring staples. In this context it was more natural to define a net region for each of these two "hook-like" features. Using these nets, we then determined whether the two staples "engaged," which we defined as conformations that satisfied the condition of reciprocal engagement: (i) Any branch of staple 2 intersects with a net from staple 1, and (ii) any branch of staple 1 intersects with a net from staple 2. If any of these conditions were not verified, then the particles simply contacted with no engagement. To compute the probability for the two staples to transition from a "free" state to a state of "engagement" p_e, we determined numerically which subset $\Omega^{(e)}$ of $\Omega^{(v)}$ led to engagement between the staples. In the example of Fig. 4a, no engagement is possible and ${\Omega^{(e)}}_A=\emptyset$. Figure 4c shows another conformation, where staple 2 is initially at point B. In this second example, there is a set of directions ${\Omega^{(e)}}_B\in {\Omega^{(v)}}_B$ where staple 2 can engage with staple 1 through its catch net 2 (see supplemental movie). Once $N=10^6$ realizations of initial conformations are considered, the probability p_e of engagement between staple 1 and 2 is then given by:

$$p_e = p_v \frac{1}{N}\sum_i^N \frac{\Omega_i^{(e)}}{\Omega_i^{(v)}} \tag{6}$$

Figure 5a shows probabilities p_e as a function of crown-leg angle. The probability of engagement is the highest in the 60–90° range, and it is zero for $\theta=0°$ and $\theta=180°$ because the catch nets have zero surfaces (in these two extreme cases, the staples are rods). The final step in the model is a random "bounce" of staple 2 from staple 1 and a calculation of the probability of this bounce to further engage the two staples, in which case the two staples are entangled. This additional step was important to capture the propensity of the particles to keep other particles trapped by entanglement. For this step, we only considered cases where the two staples are already engaged (Fig. 4d). We first defined a solid angular sector $\Omega^{(b)}$ defining the possible directions of a bounce away from the contact point. Within these directions, we then geometrically determined which directions $\Omega^{(t)}$ would take staple 2 further toward the "deepest" corner of the net region. More specifically, these translations $\vec{u}^{(t)}$ must satisfy, in three-dimensions:

$$\begin{cases} \vec{c}\cdot\vec{u}^{(t)} \geq 0 \\ \vec{l}\cdot\vec{u}^{(t)} \geq 0 \end{cases} \tag{7}$$

where $\bar{c}$ and $\bar{l}$ are vectors associated with the contours of the net, pointing towards the corner between the crown and the leg (Fig. 4d). The magnitude of these vectors is irrelevant in the determination of possible $\vec{u}^{(t)}$ vectors. This criterion provided a rich landscape of entanglement configuration which included translations $\vec{u}^{(t)}$ out of the plane of the net, enabling a small number of entangled configurations in staples with crown-leg angle greater than 90°. The probability p_{et} of transitioning from simple engagement to an entangled conformation was then compute using:

$$p_{et} = \frac{1}{N}\sum_i^N \frac{\Omega_i^{(t)}}{\Omega^{(b)}} \tag{8}$$

A supplemental movie illustrates how these probabilities are computed with the throw-bounce-tangle model.

Figure 5b shows the probability of further entanglement from an engaged configuration as a function of crown-leg angle. Once the staples are engaged, the probability of entanglement increases rapidly when angle θ is decreased. In other words, staples with smaller θ, once they engage with other staples, are much more likely to geometrically "trap" these staples. The entanglement probability between two staples, accounting for all three possible transition paths to entanglement configurations, can then be written:

$$p_t = p_e \cdot p_{et} \tag{9}$$

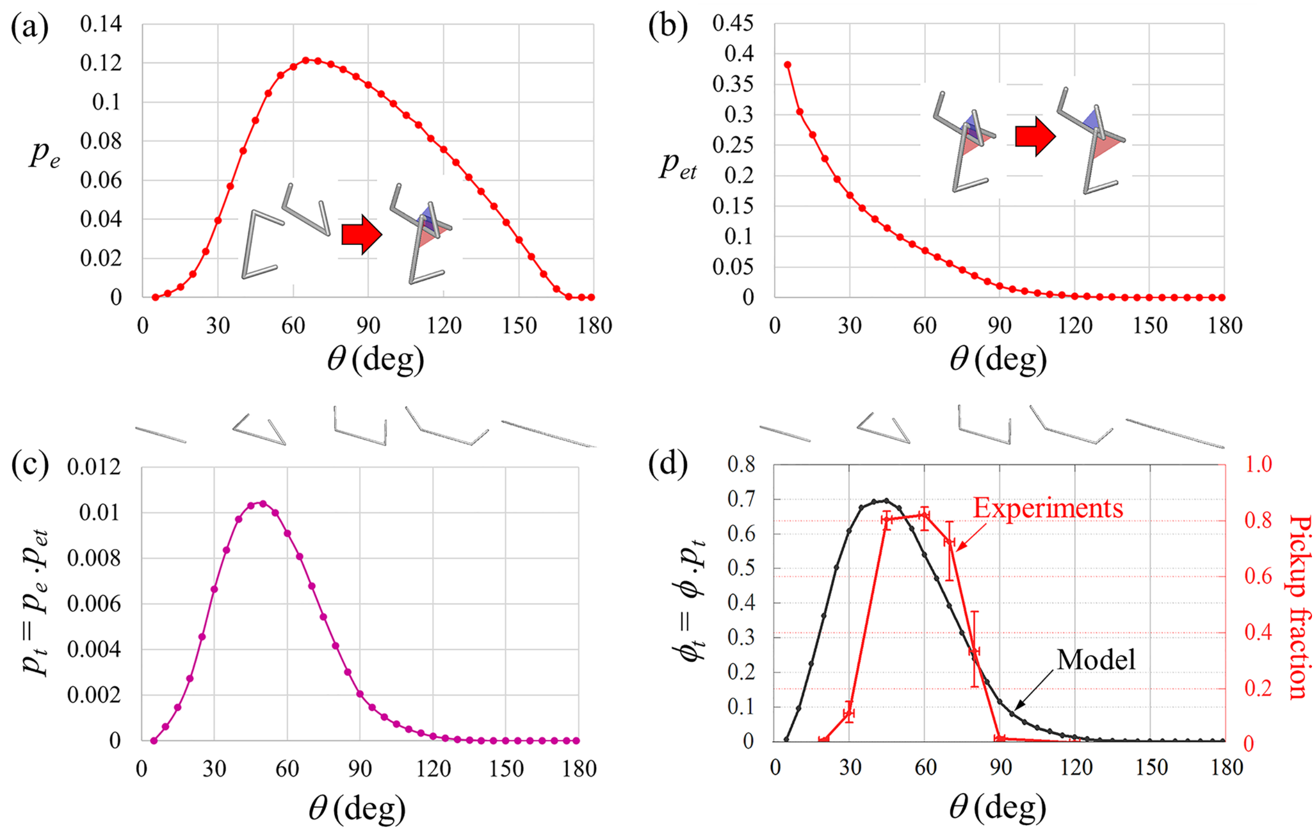

Fig. 5 Main results from the throw-bounce-tangle model for a pair of staples of different crown-leg angles θ: **a** Probability of engagement; **b** probability of transitioning from "engaged" to "entangled"; **c** probability of entanglement and **d** Volumetric density of entangled staples as a function of crown-leg angle θ (the experimental results are also shown on that plot)

Figure 5b shows the probabilities p_t as function of crown-leg angle. The model predicts an entanglement probability which is maximum at $\theta \sim 50°$ and which vanishes towards $\theta = 0°$, and $\theta = 180°$. Finally, as pointed out by Gravish et al. [26], the strength of a bundle of staples is also a function of the volume fraction of staples in the bundle. Following this model, we write the average entanglement density in the bundle, as the average number of entangled staples in a $l \times l \times l$ volume (i.e., the unit volume is expressed in unit of l):

$$\phi_t = \phi \cdot p_t \tag{10}$$

The volumetric density of entangled staples ϕ_t we use here is different from $<N>$, the average number of neighboring staples that engage with each staple in the bundle [14]. However, as illustrated below, both metrics for entanglement lead to the same predictive trends for the entanglement strength of the bundles. Figure 5d shows ϕ_t as a function of the crown leg angle θ. The packing factor ϕ is greater for staples with smaller θ, so the effect of applying Eq. (10) is a slight shift of the peak entanglement from $\theta = 50°$ for p_t to a maximum for ϕ_t at $\theta \sim 35$–$55°$. In this case, the profiles for p_t and ϕ_t are very similar (which will not be necessarily the case when other geometrical parameters of the staples will be varied in the upcoming sections of this report). Figure 5d also shows the experimental pick-up fraction as a function of crown-leg angle. The model agrees well with the experiments which showed a maximum entanglement density near $\theta = 35$–$60°$, and no entanglement as the crown-leg angle nears $\theta = 0°$ and $\theta = 180°$. This model therefore properly captures a competition of effects resulting in an optimum geometry for entanglement: (i) The density of staples is the highest for staples with low θ (Fig. 3c); (ii) Rod like staples cannot engage, and the engagement probability is the highest near $\theta = 70°$ (Fig. 5a); (iii) if they do engage, the probability of "trapping" or "entangling" other staples is higher in staples with low θ. This result suggests that this two-staple throw-bounce-tangle model can be used to predict entanglement density in a bundle of staples, and that the entanglement density, in turn, governs the strength of the bundle. In the next sections, we test the throw-bounce-tangle model against experiments on other types of staples.

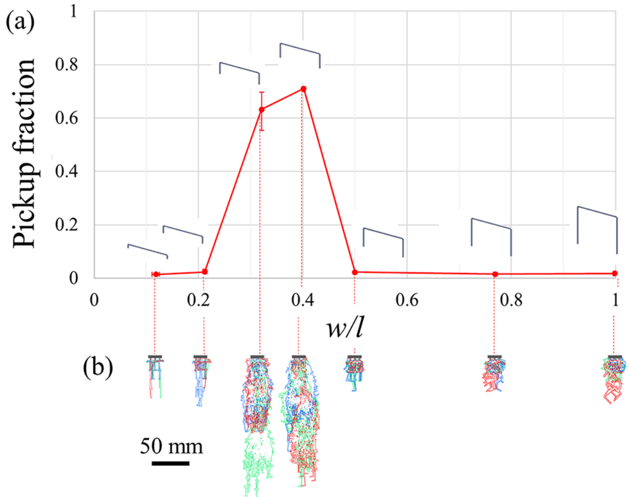

Fig. 6 Effect of leg length: **a** Experimental pick-up fraction as a function of normalized leg length *w/l*; **b** Composite images of the picked-up bundles from three experiments

4 Effects of leg length

The relative leg length *w/l* is another critical geometrical parameter in individual staples [26]. To explore this parameter experimentally, we decreased the leg lengths of standard staples by milling the legs of sticks of staples from $w = 6.35$ mm for standard staples down to 5.1 mm, 4.1 mm, 2.7 mm, or 1.5 mm. We also acquired other staples with longer legs ($w = 9.5$ mm and $w = 12.7$ mm, $d = 0.74 \times 0.59$ mm^2, Swingline, IL). Three pick-up tests were performed on bundles of 1000 staples for each of these geometries. Figure 6b shows the pick-up fraction as a function of normalized leg length *w/l*. We observed a clear peak at $w/l = 0.4$, and a sharp decrease for shorter or longer legs. Interestingly, this peak ratio *w/l* is identical to the optimum found with column-collapse experiments in Gravish et al. [26].

Figure 7a shows the volumetric density ϕ of staples measured experimentally and fitted with the model of Eq. (3). As expected, longer legs for the individual staples result to a rapid decrease in ϕ. Figure 7b-f show the results of the throw-bounce-tangle model, which recovers the competing effects discussed in Gravish et al. [26]: As leg length is increased, higher visibility and higher chances of engagement (Fig. 7b, c) result in a rapid increase of probability for

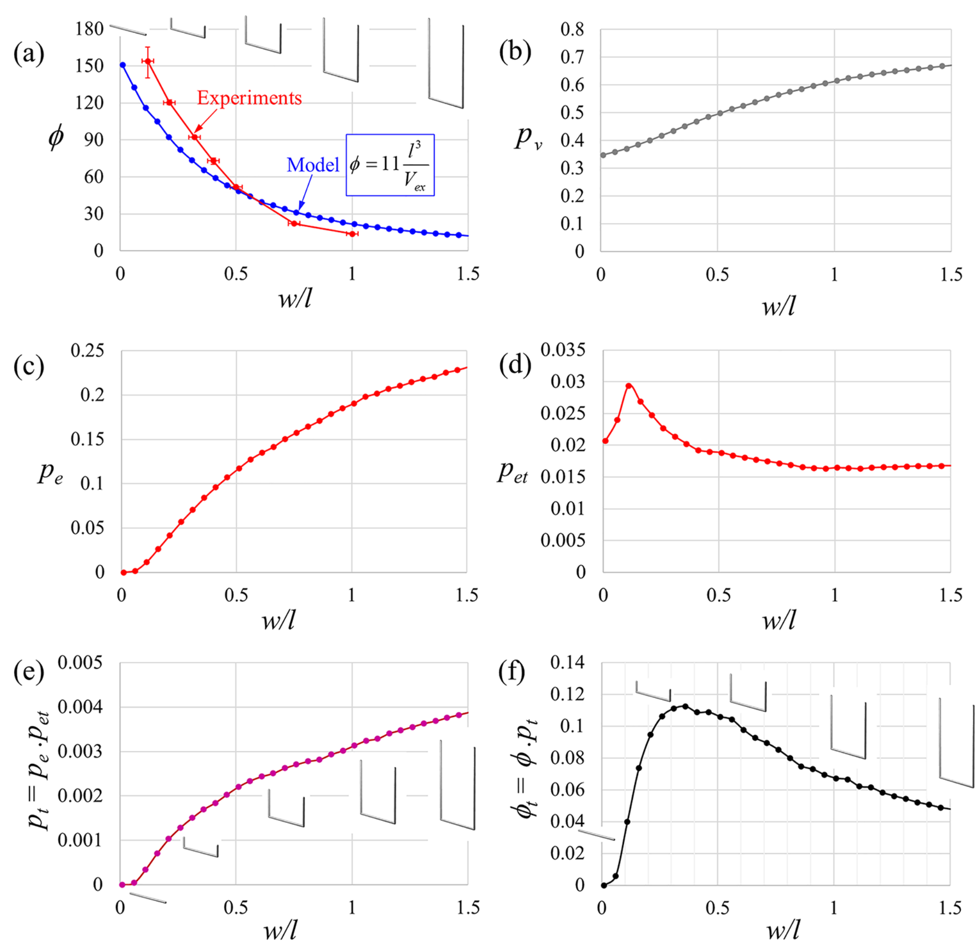

Fig. 7 Results from the throw-bounce-tangle model for a pair of staples as a function of leg length *w/l*: **a** Experimental and modeled staple volumetric density; **b** "Visibility" p_v of individual staples; **c** Probability of engagement; **d** Transition probability from engaged to entangled; **e** Overall probability of entanglement and **f** Volumetric density of entangled staples as a function of leg length *w/l*

entanglement (Fig. 7e). However longer legs also lead to a rapid decrease in ϕ (Fig. 7a), so that these two competing effects give rise to an optimum w/l value for entanglement at about $w/l=0.4$, which is in good agreement with the optimum from the experiments and with the results of Gravish et al. [14].

5 Effect of backbone thickness

Intuitively, we expected the thickness of the backbone of the staples to have minimal effects on entanglement as long as the backbone of the staples is "sufficiently thin" compared to its other dimensions. 3D printing of particles, which has been used in previous studies [16, 20], has relied on this assumption: Because of the limitations in printer resolution and material choice (polymers), 3D printed particles for entangles have backbones with larger relative cross-sections compared to steel staples. However, in preliminary experiments, we noticed that 3D printed polymeric particles did not entangle well compared to thin steel staples. In this section, we explore the effects of backbone thickness. As a reference, we used the $\theta=60°$ steel staple design described above, which has a backbone cross section $d^2=0.41\times0.48$ mm^2. We also fabricated two other designs, with a backbone contour identical to the $\theta=60°$ steel staple but with thicker backbone cross sections: $d^2=0.85\times0.85$ mm^2 and $d^2=1.50\times1.50$ mm^2. These two thicker types of staples were cut from 0.85 mm and 1.5 mm thick acrylic sheets using a precision laser cutter (Nova 35, Thunder Laser, TX). In addition to different cross sections, the stiffness and frictional properties of these acrylic staples differed from the steel staples used so far in this study, so it is useful to mention the impact of these parameters on pickup fraction. Experiments on $\theta=90°$ steel staples revealed an average pickup fraction of 0.023. The same experiments, performed on $\theta=90°$ acrylic staples, revealed a pickup fraction of 0.05. These fractions are small, because $\theta=90°$ staples produce relatively poor geometrical entanglement. In these conditions it is possible that other factors such as stiffness and friction contributed to difference in measured pickup fraction between steel and acrylic samples. On the other hand, for $\theta=60°$ staples we measured a pickup fraction of 0.82 for the steel staples and 0.84 for the acrylic staples. These numbers are quite close, suggesting that when geometrical entanglement is strong, geometrical effects largely prevail over effects of friction or deformations of the staples (at least in a regime where stresses are relatively low: recent work on tensile tests on bundles of staples have shown that friction and staple deformability must be taken into account when tensile stresses are high [19]). We now focus on the effect of backbone thickness. The pick-up tests revealed a sharp decrease in entanglement for thicker staples (Fig. 8): Doubling the thickness of the backbone from $d/l=0.035$ to $d/l=0.065$ resulted in a 75% decrease in pick-up ratio, even though the backbones in these cases may still be considered "thin" ($d/l<<1$).

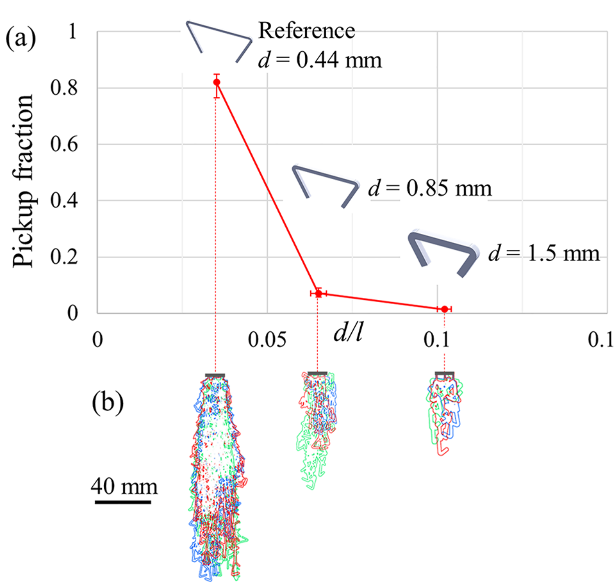

Fig. 8 Effect of backbone thickness: **a** Experimental pick-up fraction as a function of normalized backbone thickness d/l; **b** Composite images of the picked-up bundles

Figure 9 shows the results of the throw-bounce-tangle simulations. Except for the probabilities of entanglement from engagement p_{et}, all characteristics decrease with d/l. This includes the volumetric density, which appears to converge to infinity in the $d/l=0$ limit. Indeed, as the cross section of the staples converges to zero no collision can be detected, so that the excluded volume converges to zero and the volumetric density of staples converges to infinity. This effect largely explains how the entanglement density ϕ_t decreases rapidly when the backbone thickness d/l is increased, in accordance with the experimental results. The model therefore reveals the main two contributors of the poor entanglement density ϕ_t for staples with thicker backbones: Decreased staple density ϕ, and decreased probabilities of engagement p_e.

6 Effect of twisting

Experiments on 3D-printed staple-like particles have shown that entanglement and strength can also be manipulated by twisting the staples about the axis of the crown [20]. In this final section, we examine the effect of twisting the legs of individual staples. As a reference, we used the $\theta=90°$ and 60° steel staples described above. For each of these angles, we explored two twisted designs: A set of staples twisted

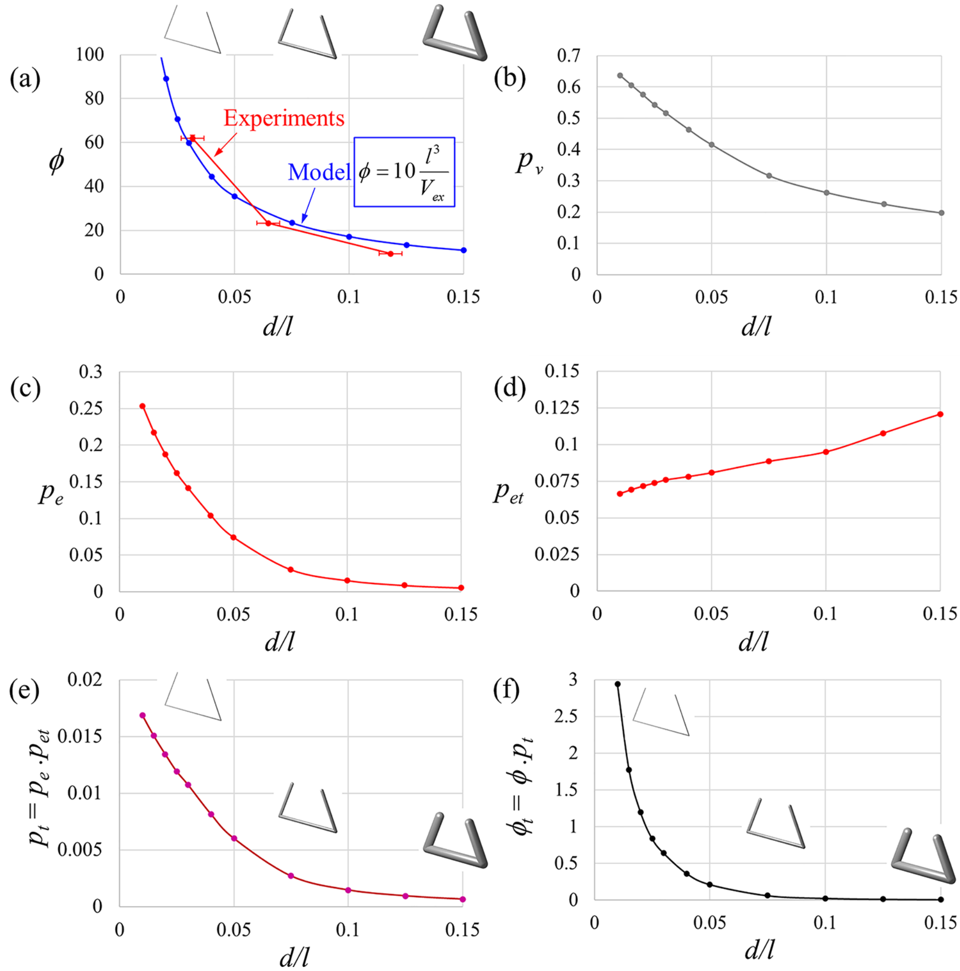

Fig. 9 Results from the throw-bounce-tangle model for a pair of staples as a function of backbone thickness *d*/*l*: **a** Experimental and modeled staple volumetric density; **b** "Visibility" p_v of individual staples; **c** Probability of engagement; **d** Transition probability from engaged to entangled; **e** Overall probability of entanglement and **f** Volumetric density of entangled staples as a function of backbone thickness *d*/*l*

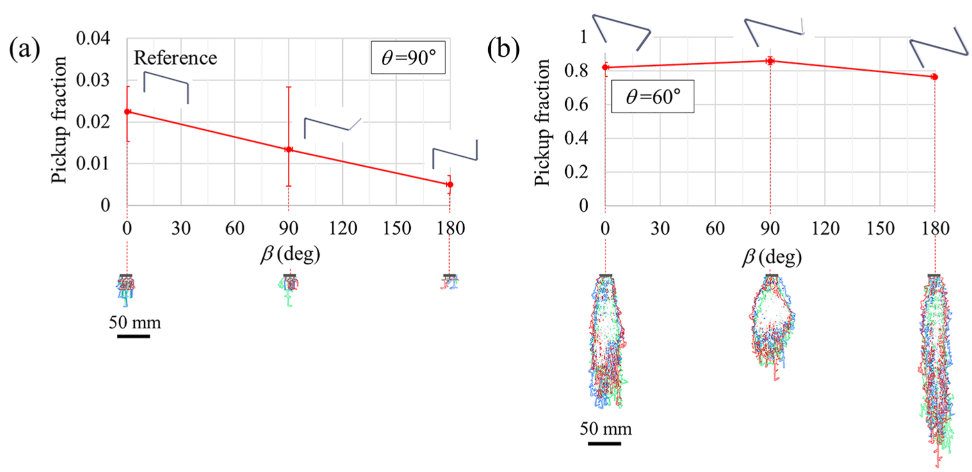

Fig. 10 Effect of twisting staples: Experimental pick-up fraction as a function of twist angle β for staples with **a** θ=90° and **b** θ=60°

by an angle β=90° about the axis of the crown, and another set of staples twisted by an angle β=180° about the axis of the crown (Fig. 10a, b). Individual staples were manually twisted about the axis of the crown, resulting in permanent change of geometry from plastic deformations. Figure 10a shows the results for θ=90° staples: Twisting angle had almost no effects on the pick-up fraction. However, any possible effect might be obscured by the already very low pick-up fraction for θ=90° staples (0.02). The results for the twisted, θ=60° staples (Fig. 10b) show a slightly more pronounced effect of twisting: Compared to the reference staple (β=0°), entanglement increases by about 3.9% in staple twisted to β=90°, but that entanglement degrades to below reference values for β=180°. We however noticed that the

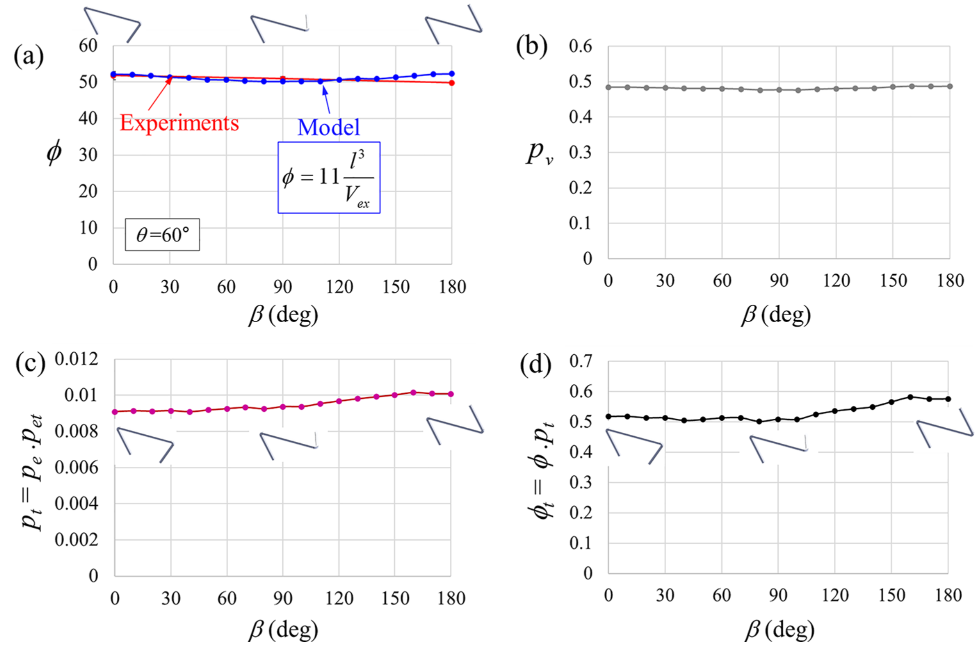

Fig. 11 Results from the throw-bounce-tangle model for a pair of staples as a function of angle of twist β, for cases where staple distribution is fully isotropic: **a** Experimental and modeled staple volumetric density; **b** "Visibility" p_v of individual staples; **c** Probability of entanglement and **d** Volumetric density of entangled staples

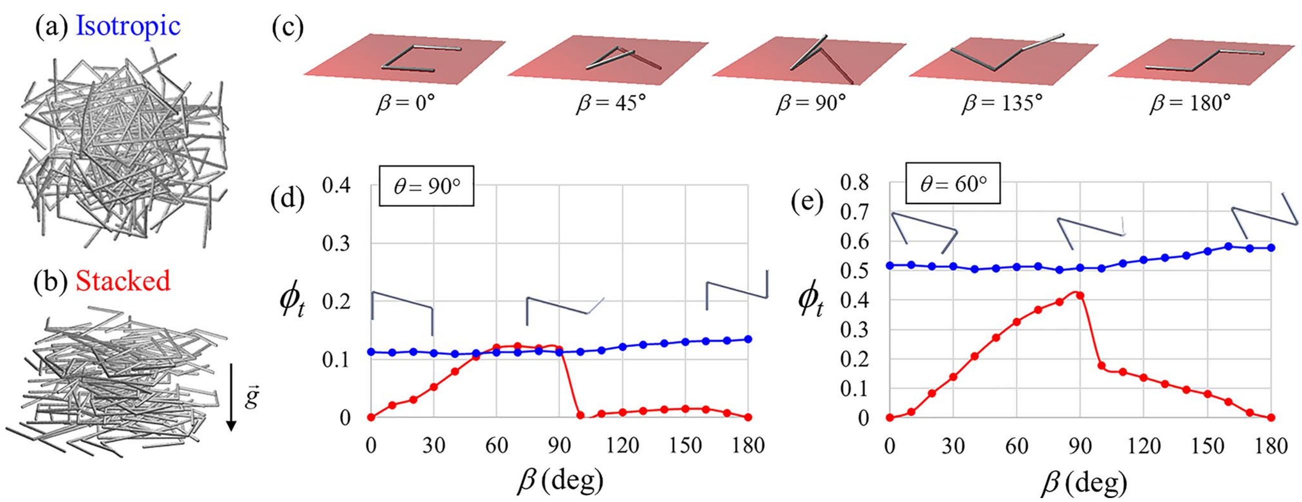

Fig. 12 Effect of stacking or "pancaking": **a** In the isotropic case the orientation of the staples is fully random; **b** In the stacked or "pancaked" case, the backbones of the staples align across the direction of gravity; **c** Stacked staples with various angles of twist β. When β = 0° or β = 180°, all branches of the staples are in the horizontal plane, making entanglement impossible. In other cases, legs coming out of the plane make entanglement across staked planes possible; Density of entanglement as a function of twist angle β for **d** staples with θ = 90° and **e** staples with θ = 60°

picked bundle for the β = 90° case was more "compact" (i.e. less elongated vertically) than for β = 0° and β = 180°, a possible indication of better entanglement stability.

Figure 11 shows the results from the throw-bounce-tangle model using fully isotropic orientations for the staples, which predicts a very modest effect of twist angle β on every measure of density and probabilities.

Murphy et al. [20] explained the benefits of twisted staples for entanglement in the context of what they term a "pancaking" effect: Under the combined effects of vibration and gravity, the crown and the legs of the staples tend to align on stacked horizontal planes perpendicular to gravity (Fig. 12a). When β = 0° or β = 180°, all branches of the staples are in the horizontal plane, making entanglement impossible (Fig. 12b). In other intermediate cases (0 < β < 180°), legs coming out of the horizontal plane make entanglement possible across stacked planes. We captured this "stacking" or "pancaking effect" effect in our model by introducing a bias on the orientation of staples 1 and 2: When we numerically created staple 1 and 2, we required that (i) the crowns of both staples 1 and 2 lie in a horizontal and (ii) the sum of the absolute values of angles between the legs and the horizontal to be minimized, in order to simulate the propensity of the legs to also align across the direction of gravity

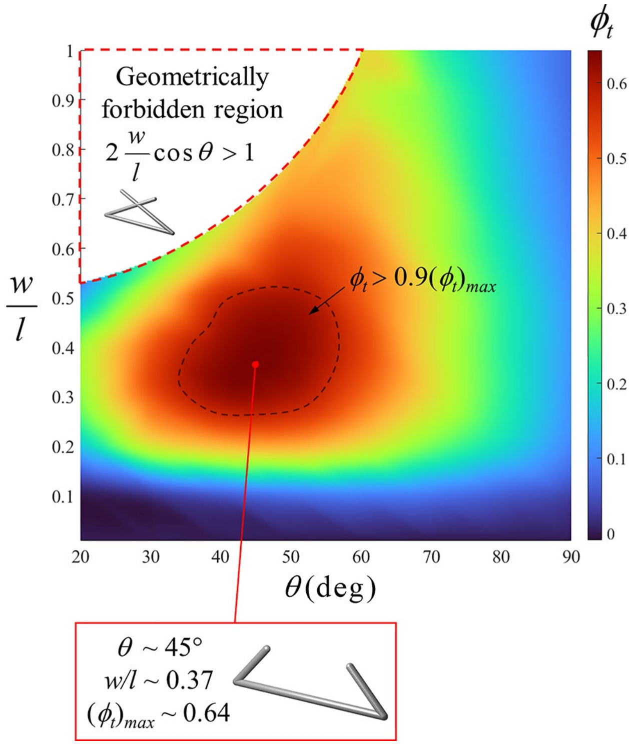

Fig. 13 Map of entanglement density as a function of crown leg angle and leg length. The map reveals an optimum design at $\theta \sim 45°$ and $w/l \sim 0.37$. A broad range of designs in the neighborhood of the optimum also performs very well in terms of entanglement, with $\phi_t > 0.9(\phi_t)_{max}$

[20]. Figure 12b shows examples of staple alignment for staples with different twist angles β. As the twist angle is increased from $\beta = 0°$–$90°$, the legs protrude more and more from either side of the horizontal plane. At $\beta > 90°$ there is a sharp transition, with the legs protruding from only one side of the plane (to satisfy condition (ii) above), and the out-of-plane protrusions decreasing progressively up to $\beta = 180°$. Figure 12c, d show the predictions of the throw-bounce-tangle model: Compared to the isotropic case, stacking generally decreases the density of entanglement. However, in these stacked staples, the density of entanglement becomes a strong function of the twist angle β. In $\beta = 90°$ and $\beta = 180°$ cases, the legs are in the horizontal plane and no engagement and entanglement are possible between staple 1 and 2. In other twisted geometries, the legs of staple 1 and 2 are out-of-plane, which greatly increased the likelihood of entanglement, with a clear maximum at $\beta = 90°$, which is consistent with our experiments and the experiments in [20]. Finally, we note that the sharp drop in entanglement predicted for $\beta > 90°$ is explained by both of the legs being on the same side of the horizontal plane, an outcome of enforcing condition (ii) above.

7 An optimum staple geometry

The sections above have shown that the throw-bounce-tangle model can capture variations of entanglement for different staple geometries, in ways which are consistent with experiments and with previous studies. Because this model is relatively simple and computationally efficient, it is amenable to the exploration of large numbers of possible staple designs. In this section, we give such example, where we explore the crown leg angle–leg length ($\theta - w/l$) design space. We performed a "brute force" exploration of the design space by considering ~5000 combinations of these parameters over a range of $20° < \theta < 120°$ and $0 < w/l < 1.5$. The combinations of these parameters that would lead to the legs of the staples crisscrossing (for which $2(w/l)\cos\theta > 1$) were excluded from this exploration. Figure 13 shows a map of entanglement density as a function of θ and w/l. The map reveals a single maximum entanglement density for $\theta \sim 45°$ and $w/l \sim 0.37$, but the landscape in the design space is quite smooth, and that optimum peak is not particularly sharp. For example, deviations as large as 10–20% from the optimum values for w/l and θ only result in a 10% loss of entanglement density (black dotted contour on Fig. 13). This result is advantageous in terms of design robustness, because defects and deviations from the optimum geometry would still result in high entanglement. The optimum geometry identified in this map is very close to one of the staple designs tested in this report (Fig. 2). Indeed, the experimental pick-up ratio for that design ($\theta = 45°$ and $w/l = 0.37$) was the highest we measured in this study.

8 Conclusions

Entangled matter provides intriguing perspectives in terms of deformation mechanisms, mechanical properties, assembly, and disassembly. Collective entanglement mechanisms are complex, occur over multiple length scales, and they are not fully understood to this day. In this report, we propose a simple pick-up test which can be used as a metric for entanglement. This method produces results which are consistent with other, more complicated experimental methods previously proposed to measure entanglement [15, 20, 26]. We also presented a new "throw-bounce-tangle" model, which is based on a 3D geometrical entanglement criterion between two staples, and a Monte Carlo numerical approach to extract probabilities of entanglement. This relatively simple model predicts an average density of entanglement, and it recovers the trends and optimum staple geometries identified experimentally: Entanglement can be manipulated by tuning the leg-to-crown ratio, the crown-lag angle, and the twist angle. We also show, using experiments and our model, that entanglement is very sensitive to the thickness of the backbone of the staples, even in regimes where that thickness is a small fraction (<0.04) of the other dimensions. Staples with thin backbones promote entanglement, and it is probably possible to manufacture such staples. However, a potential issue for exceedingly "thin" staples would probably be large deformations or even failure due to their reduced cross sections. While the "throw-bounce-tangle" model is simple and can predict basic trends in entangled matter, this model does not consider geometrical hindrance in large bundles, the deformation of individual particles, frictional effects, or longer-range effects such as the formation and evolution of force lines. Consideration of these effects would probably improve the accuracy of predictions, but would require careful experimental validations including measures of order and disorder in the bundle. In the experiments presented here, bundles of staples were subjected to gravity forces only, which generated relatively low stresses and deformations. From what is known from previous studies [15, 16] and from our own experiments and models on tensile behavior of entangled staples [19], the formation and evolution of force lines may play a more important role in bundles of staples subjected to high tensile stresses and large deformation (>100% strain). With these limitations in mind, the "throw-bounce-tangle" model still provides good estimates for the propensity of particle to entangle, and it can be used for the design and optimization of staple-like particles. In this report we demonstrate that the crown leg angle– leg length design space can be explored exhaustively using brute force to identify optimum particle designs. The smoothness of the design landscape makes it amenable to computationally efficient gradient-based optimization methods. The "throw-bounce-tangle" could also be used in the future to explore more complex three-dimensional designs, for example branched particles with barbs and a multitude of geometrical nets. For these particles the model may need to be expanded to account for cases where more than two particles are involved to generate entanglement strength. In terms of loading conditions, the results presented here show that our model captures the strength of entangle bundles subjected to gravity (original pick-up experiments presented here), vibration/gravity [14] and flexural bending [20]. A parallel project we are conducing on bundles of staples under tensile deformations shows that when the crown-leg angle is changed, the tensile strength (measured from tensile tests) varies in ways similar to what is reported here [19]. This body of experiments suggest that our model is versatile in terms of predicting strength under different loading modes, although more experiments would be required to confirm the generality of the model. Geometric entanglement can also be exploited in microscale [28] or even nanoscale particles [29]. Interestingly, the entangled matter is prominent in nature, in the form of "passive entanglement" in bird nests [30, 31], beaver dams [32, 33], seed barbs and hooks attachments [34, 35] and also "active entanglement" in ant rafts [36, 37] or worm blobs [38]. The model presented here, applied to these natural systems, could lead to a better understanding of how they produce strength and mechanical stability. These systems could also, in turn, provide a rich source of inspiration for new entangled materials. Along this line of bio-inspiration, the models can be adapted, in the future, to active entangled matter where particle can change their shape and entanglement capabilities dynamically [22]. New optimized designs for individual particles may produce entangled bundles with attractive combinations of strength, extensibility, and toughness that may soon outperform lightweight engineering materials such as solid foams and lattices.

Supplementary Information The online version contains supplementary material available at https://doi.org/10.1007/s10035-025-01531-w.

Acknowledgements This work was supported by the US National Science Foundation (Mechanics and Materials and Structures, Award No. 2033991). YS was also partially supported by the Department of Mechanical Engineering at the University of Colorado.

Author contributions Conceptualization: YS, SP, FB; Investigation: YS; Methodology: YS, FB; Writing-original draft: YS; Writing-review and editing: YS, SP, FB; Formal Analysis: YS, FB; Supervision: FB.

Data availability No datasets were generated or analysed during the current study.

Declarations

Conflict of interest The authors declare that they have no conflict of interest.

Ethical approval Not applicable.

References

1. Behringer, R.P., Chakraborty, B.: The physics of jamming for granular materials: a review. Rep. Prog. Phys. (2018). https://doi.org/10.1088/1361-6633/aadc3c
2. Jaeger, H.M.: Celebrating soft matter's 10th anniversary: toward jamming by design. Soft Matter (2015). https://doi.org/10.1039/C4SM01923G
3. Murphy, K.A., MacKeith, A.K., Roth, L.K., Jaeger, H.M.: The intertwined roles of particle shape and surface roughness in controlling the shear strength of a granular material. Granular Matter (2019). https://doi.org/10.1007/s10035-019-0913-7
4. Gans, A., Pouliquen, O., Nicolas, M.: Cohesion-controlled granular material. Phys. Rev. E (2020). https://doi.org/10.1103/PhysRevE.101.032904
5. Karuriya, A.N., Simoes, J., Barthelat, F.: Fully dense and cohesive fcc granular crystals. Extr. Mech. Lett. (2024). https://doi.org/10.1016/j.eml.2024.102208
6. Philipse, A.P.: The random contact equation and its implications for (colloidal) rods in packings, suspensions, and anisotropic powders. Langmuir (1996). https://doi.org/10.1021/la950671o
7. Wouterse, A., Luding, S., Philipse, A.P.: On contact numbers in random rod packings. Granular Matter (2009). https://doi.org/10.1007/s10035-009-0126-6
8. Blouwolff, J., Fraden, S.: The coordination number of granular cylinders. Europhys. Lett. (2006). https://doi.org/10.1209/epl/i2006-10376-1
9. Jung, Y., Plumb-Reyes, T., Lin, H.-Y.G., Mahadevan, L.: Entanglement transition in random rod packings. arXiv (2023). https://doi.org/10.48550/arXiv.2310.04903
10. Barés, J., Zhao, Y., Renouf, M., Dierichs, K., Behringer, R.: Structure of hexapod 3d packings: understanding the global stability from the local organization. EPJ Web Conf. (2017). https://doi.org/10.1051/epjconf/201714006021
11. Aponte, D., Estrada, N., Barés, J., Renouf, M., Azéma, E.: Geometric cohesion in two-dimensional systems composed of star-shaped particles. Phys. Rev. E (2024). https://doi.org/10.1103/PhysRevE.109.044908
12. Cantor, D., Cárdenas-Barrantes, M., Orozco, L.F.: Bespoke particle shapes in granular matter. Pap. Phys. (2022). https://doi.org/10.4279/pip.140007
13. Dierichs, K., Menges, A.: Towards an aggregate architecture: designed granular systems as programmable matter in architecture. Granular Matter (2016). https://doi.org/10.1007/s10035-016-0631-3
14. Gravish, N., Franklin, S.V., Hu, D.L., Goldman, D.I.: Entangled granular media. Phys. Rev. Lett. (2012). https://doi.org/10.1103/PhysRevLett.108.208001
15. Franklin, S.V.: Extensional rheology of entangled granular materials. Europhys. Lett. (2014). https://doi.org/10.1209/0295-5075/106/58004
16. Karapiperis, K., Monfared, S., Macedo, R.B.D., Richardson, S., Andrade, J.E.: Stress transmission in entangled granular structures. Granular Matter (2022). https://doi.org/10.1007/s10035-022-01252-4
17. Marschall, T.A., Franklin, S.V., Teitel, S.: Compression-and shear-driven jamming of u-shaped particles in two dimensions. Granular Matter (2015). https://doi.org/10.1007/s10035-014-0540-2
18. Zhao, Y., Barés, J., Socolar, J.E.: Yielding, rigidity, and tensile stress in sheared columns of hexapod granules. Phys. Rev. E (2020). https://doi.org/10.1103/PhysRevE.101.062903
19. Pezeshki, S., Sohn, Y., Fouquet, V., Barthelat, F.: Tunable entanglement and strength with engineered staple-like particles: experiments and discrete element models. J. Mech. Phys. Solids (2025). https://doi.org/10.1016/j.jmps.2025.106127
20. Murphy, K.A., Reiser, N., Choksy, D., Singer, C.E., Jaeger, H.M.: Freestanding loadbearing structures with z-shaped particles. Granular Matter (2016). https://doi.org/10.1007/s10035-015-0600-2
21. Murphy, K., Roth, L., Peterman, D., Jaeger, H.: Aleatory construction based on jamming: stability through self-confinement. Archit. Des. (2017). https://doi.org/10.1002/ad.2198
22. Savoie, W., Tuazon, H., Tiwari, I., Bhamla, M.S., Goldman, D.I.: Amorphous entangled active matter. Soft Matter (2023). https://doi.org/10.1039/D2SM01573K
23. Trepanier, M., Franklin, S.V.: Column collapse of granular rods. Phys Rev E—Stat, Nonlinear Soft Matter Phys, (2010). https://doi.org/10.1103/PhysRevE.82.011308
24. Govender, N., Wilke, D.N., Wu, C.-Y., Khinast, J., Pizette, P., Xu, W.: Hopper flow of irregularly shaped particles (non-convex polyhedra): Gpu-based dem simulation and experimental validation. Chem. Eng. Sci. (2018). https://doi.org/10.1016/j.ces.2018.05.011
25. Li, L., Marteau, E., Andrade, J.E.: Capturing the inter-particle force distribution in granular material using ls-dem. Granular Matter (2019). https://doi.org/10.1007/s10035-019-0893-7
26. Gravish, N., Goldman, I.D.: Entangled granular media. In: Fernandez-Nieves, A., Puertas, A.M. (eds.) Fluids, colloids and soft materials - an introduction to soft matter physics, pp. 341–354. Wiley, Hoboken (2016)
27. The Math Works Inc: Matlab version: 9.13.0 (r2022b). (2022). https://www.mathworks.com
28. Paulsen, K.S., Deng, Y., Chung, A.J.: Diy 3d microparticle generation from next generation optofluidic fabrication. Adv. Sci. (2018). https://doi.org/10.1002/advs.201800252
29. Miszta, K., De Graaf, J., Bertoni, G., Dorfs, D., Brescia, R., Marras, S., Ceseracciu, L., Cingolani, R., Van Roij, R., Dijkstra, M.: Hierarchical self-assembly of suspended branched colloidal nanocrystals into superlattice structures. Nat. Mater. (2011). https://doi.org/10.1038/nmat3121
30. Weiner, N., Bhosale, Y., Gazzola, M., King, H.: Mechanics of randomly packed filaments—the "bird nest" as meta-material. J. Appl. Phys. (2020). https://doi.org/10.1063/1.5132809
31. Bhosale, Y., Weiner, N., Butler, A., Kim, S.H., Gazzola, M., King, H.: Micromechanical origin of plasticity and hysteresis in nestlike packings. Phys. Rev. Lett. (2022). https://doi.org/10.1103/PhysRevLett.128.198003
32. Żurowski, W.: Building activity of beavers. Acta Theriol. (1992). https://doi.org/10.4098/AT.ARCH.92-41
33. Larsen, A., Larsen, J.R., Lane, S.N.: Dam builders and their works: beaver influences on the structure and function of river corridor hydrology, geomorphology, biogeochemistry and ecosystems. Earth-Sci. Rev. (2021). https://doi.org/10.1016/j.earscirev.2021.103623
34. Claus, C.G., Gorb, E.V., Gorb, S.N., Li, C.: Comparative study on mechanical properties and biomineralization of hooks in the diaspores of three epizoochorous plant species. Acta Biomater. (2024). https://doi.org/10.1016/j.actbio.2024.07.041
35. Sorensen, A.E.: Seed dispersal by adhesion. Annu. Rev. Ecol. Syst. (1986). https://www.jstor.org/stable/2097004
36. Hu, D., Phonekeo, S., Altshuler, E., Brochard-Wyart, F.: Entangled active matter: from cells to ants. Eur. Phys. J.: Spec. Top. (2016). https://doi.org/10.1140/epjst/e2015-50264-4
37. Phonekeo, S., Dave, T., Kern, M., Franklin, S.V., Hu, D.L.: Ant aggregations self-heal to compensate for the ringelmann effect. Soft Matter (2016). https://doi.org/10.1039/C6SM00063K

38. Worley, A., Sendova-Franks, A.B., Franks, N.R.: Social flocculation in plant–animal worms. R. Soc. Open Sci. (2019). https://doi.org/10.1098/rsos.181626